

Contaminated Multivariate Time-Series Anomaly Detection with Spatio-Temporal Graph Conditional Diffusion Models

Thi Kieu Khanh Ho and Narges Armanfard*,

Department of Electrical and Computer Engineering, McGill University
Mila - Quebec AI Institute, Montreal, QC, Canada

Abstract

Mainstream unsupervised anomaly detection algorithms often excel in academic datasets, yet their real-world performance is restricted due to the controlled experimental conditions involving clean training data. Addressing the challenge of training with noise, a prevalent issue in practical anomaly detection, is frequently overlooked. In a pioneering endeavor, this study delves into the realm of label-level noise within sensory time-series anomaly detection (TSAD). This paper presents a novel and practical end-to-end unsupervised TSAD when the training data is contaminated with anomalies. The introduced approach, called TSAD-C, is devoid of access to abnormality labels during the training phase. TSAD-C encompasses three core modules: a Decontaminator to rectify anomalies (aka noise) present during training, a Long-range Variable Dependency Modeling module to capture long-term intra- and inter-variable dependencies within the decontaminated data that is considered as a surrogate of the pure normal data, and an Anomaly Scoring module to detect anomalies from all types. Our extensive experiments conducted on four reliable and diverse datasets conclusively demonstrate that TSAD-C surpasses existing methodologies, thus establishing a new state-of-the-art in the TSAD field.

1. Introduction

Multivariate time-series data (MTS) is referred to as time-stamped data that consists of multiple variables, i.e., for each timestamp, there are multiple values associated with it. Time-series anomaly detection (TSAD) is the process of detecting unusual patterns or events within time-series data that deviate from the expected behavior (Schmidl, Wenig, and Papenbrock 2022). The unusual patterns can be found in many real-world applications such as financial fraud, abrupt temperature spikes, security breaches, system malfunctions, and irregularities in brain activities. Many algorithms have been proposed to automatically detect anomalies in MTS (Su et al. 2019; Audibert et al. 2020; Deng and Hooi 2021; Li et al. 2021; Chen et al. 2022; Carmona et al. 2022; Yang et al. 2023; Ho and Armanfard 2023; Chen et al. 2024). However, several critical challenges remain unresolved.

First, existing studies can be categorized into two groups, which are supervised methods utilizing both labeled nor-

mal and abnormal data during training, and unsupervised methods assuming that only normal data is available during training. Given the demanding nature of accurately labeling anomalous patterns – proving to be time-consuming, costly, and labor-intensive – supervised approaches are deemed impractical. Thus, there has been a recent surge in the development of unsupervised approaches. However, in real-world applications, anomalies often sneak into normal data, which come from the data shift or human misjudgment (Jiang et al. 2022). These unsupervised methods are sensitive to the seen anomalies due to their exhaustive strategy to model the normal training data, hence, they would misdetect similar anomaly samples in the test phase. Therefore, developing a method that can detect anomalies while being trained on contaminated data is necessary, yet there is no method that has aimed to tackle this challenge in the TSAD field (i).

Second, it is important to capture both intra-variable (aka temporal) and inter-variable (aka spatial) dependencies in MTS (Ho, Karami, and Armanfard 2023). However, existing unsupervised studies are unable to effectively capture them. Regarding the intra-variable dependencies, they often pre-processed data by segmenting the signals into short time intervals (Strodthoff et al. 2020; Pradhan, He, and Jiang 2022), or applied conventional networks such as recurrent neural networks or transformers (Lim et al. 2021; Katharopoulos et al. 2020). Such learned dependencies imply that observations close to each other are expected to be similar. This is problematic as trends, seasonality and unpredictability are always present in MTS. Thus, developing a method that can handle the *long-range* intra-variable dependencies to aid in distinguishing normal and abnormal variations is crucial (ii).

Regarding the inter-variable dependencies, very recently, graphs have brought the potential to model the relationships between variables (sensors) in MTS. By representing variables as nodes and their connections as edges, graphs provide an intuitive way to understand the underlying relationships between variables - a useful property in TSAD. For example, the changes in one variable can be used to predict the changes in another if they are correlated. However, modeling graphs to effectively capture this dependency type is challenging. Existing studies proposed to pre-define graphs based on prior knowledge, e.g., the known locations of sensors (Tang et al. 2021). However, in many real-world applications, pre-defining the graph properties such as node loca-

*This paper has been submitted for possible publication. Copyright may be transferred without notice, after which this version may no longer be accessible.

tions and features is not practical due to dynamic testing environments – e.g., electroencephalogram sensor locations in comatose/epilepsy patients may vary depending on the brain damaged regions. Hence, instead of pre-defining graphs, dynamically learning the graph over time is highly desirable.

Lastly, while long-range intra- and inter-variable dependencies are both important for TSAD, designing an effective joint learning framework to capture them is yet challenging. Recent studies have shown that there are two groups of a combined model: time-and-graph and time-then-graph (Gao and Ribeiro 2022). The time-and-graph approach first constructs graphs and then embeds a temporal network, while the time-then-graph approach first projects the data to a temporal network, then uses the extracted temporal features to model graphs. Compared to the former approach, the time-then-graph approach has shown significant improvement in classification and regression tasks (Gao and Ribeiro 2022; Tang et al. 2023). Yet, till now, no study has explored the time-then-graph framework for unsupervised TSAD (iii).

Based on the above observations, we propose a novel approach, called TSAD-C, that addresses (i)-(iii) challenges. The main contributions of this paper are as follows:

- We propose a novel *fully* unsupervised approach, namely TSAD-C, trained on contaminated data in an end-to-end manner to detect anomalies in MTS. To the best of our knowledge, this is the first study that uses contaminated data in the training phase for TSAD, addressing a much more challenging problem than the existing studies.
- TSAD-C is comprised of three core modules, namely Decontaminator, Long-range Variable Dependency Modeling, and Anomaly Scoring. The initial module aims to identify and eliminate abnormal patterns that are likely to be anomalies. This step results in the decontaminated data, which is prepared swiftly for subsequent modules. The second module is a time-then-graph approach that is designed to model the long-term intra- and inter-variable dependencies within the decontaminated data. The last module computes anomaly scores to detect anomalies.
- The novel Decontaminator employs masking strategies and a structure state space (S4)-based conditional diffusion model, while the Long-range Variable Dependency Modeling module integrates Intra-variable Modeling, and Inter-variable Modeling components. The Anomaly Scoring module leverages insights of the two modules.
- Extensive experiments on four reliable and diverse datasets demonstrate that our method outperforms prior studies, thus establishes a new state-of-the-art in the field.

2. Proposed Method

A dataset is defined as $X = (\mathbf{x}_{(1)}, \mathbf{x}_{(2)}, \dots, \mathbf{x}_{(N)})$, where $\mathbf{x}_{(i)} = (x_{(i)}^1, x_{(i)}^2, \dots, x_{(i)}^K)$ is the i th observation in the time series of N observations, $\mathbf{x}_{(i)} \in \mathbb{R}^{K \times L}$, K and L denote the number of variables (sensors) and the length of the i th observation, respectively. An observation can be conceptualized as L samples collected from K sensors over the i th time interval. Our task is to detect anomalous observations from all

types in the test data X_{test} by training the model with contaminated data X_{train} . No information about anomalies that contaminate normal data is provided during training, such as their labels or their positions within the time series. A validation set X_{valid} is used for early stopping and finding the decision threshold. The block diagram of the proposed TSAD-C method, depicting the three modules, namely Decontaminator, Long-range Variable Dependency Modeling, and Anomaly Scoring, is shown in Figure 1.

2.1. Decontaminator

This module incorporates masking strategies and an S4-based conditional diffusion model. As no information about anomalies is provided during training, we propose masking strategies to decontaminate the input data. The diffusion model is then deployed to rectify anomalies, with S4 - a noise estimator included to ensure that long-range intra-variable dependencies are effectively captured. Notably, we introduce a pioneering concept in the diffusion field, i.e., minimizing the noise error on masked portions for a simpler and more streamlined training process. The decontaminated data is then obtained by a *single* step during the reverse process, which is a fast data preparation for subsequent modules – a significant advantage for practical applications.

Masking Strategies. Following the practical scenarios, we assume that normal samples significantly outnumber anomalies. When masking a portion of X_{train} , both normal and abnormal patterns might be removed. Since normal data predominates in X_{train} , omitting some normal patterns is not likely to yield detrimental consequences as the substantial amount of remaining normal data can compensate for masked portions. Conversely, masking can help reducing the proportion of anomalies. This benefits the downstream module as it facilitates the learning process of variable dependencies that characterize the underlying behavior of normality.

We define a mask as $\mathbf{v} \in \{0, 1\}$, $\mathbf{v} \in \mathbb{R}^{K \times L}$, where zeros and ones denote the values to be masked and the values to be kept, respectively. Hence, the i th masked observation is $\mathbf{x}_{(i)}^u = \mathbf{x}_{(i)} \odot \mathbf{v}$, where $\mathbf{x}_{(i)}^u \in \mathbb{R}^{K \times L}$ and \odot denotes point-wise multiplication. We perform three masking scenarios, namely random masking (RandM), random block masking (RandBM) and blackout masking (BoM) (Alcaraz and Strothoff 2022). We control the masking ratio by the hyperparameter r , which specifies the number of timestamps to be masked. RandM randomly samples r to be masked across variables. In RandBM, there might be no time overlap between the masked windows across variables, whereas in BoM, the same time window is masked across all variables. Note that each masked window has the size of r .

S4-based Conditional Diffusion Model. This is developed based on a diffusion model (Croitoru et al. 2023) that includes the diffusion and reserve processes. In this paper, the diffusion process incrementally adds Gaussian noise to the initial stage of $\mathbf{x}_{(i)}^u$, called $\mathbf{x}_{(i)}^0$, over T diffusion steps:

$$p(\mathbf{x}_{(i)}^1, \dots, \mathbf{x}_{(i)}^T | \mathbf{x}_{(i)}^0) = \prod_{t=1}^T p(\mathbf{x}_{(i)}^t | \mathbf{x}_{(i)}^{t-1}), \quad (1)$$

where $p(\mathbf{x}_{(i)}^t | \mathbf{x}_{(i)}^{t-1}) := \mathcal{N}(\mathbf{x}_{(i)}^t; \mu_{(i)}^t, \sigma_{(i)}^t)$. This indicates

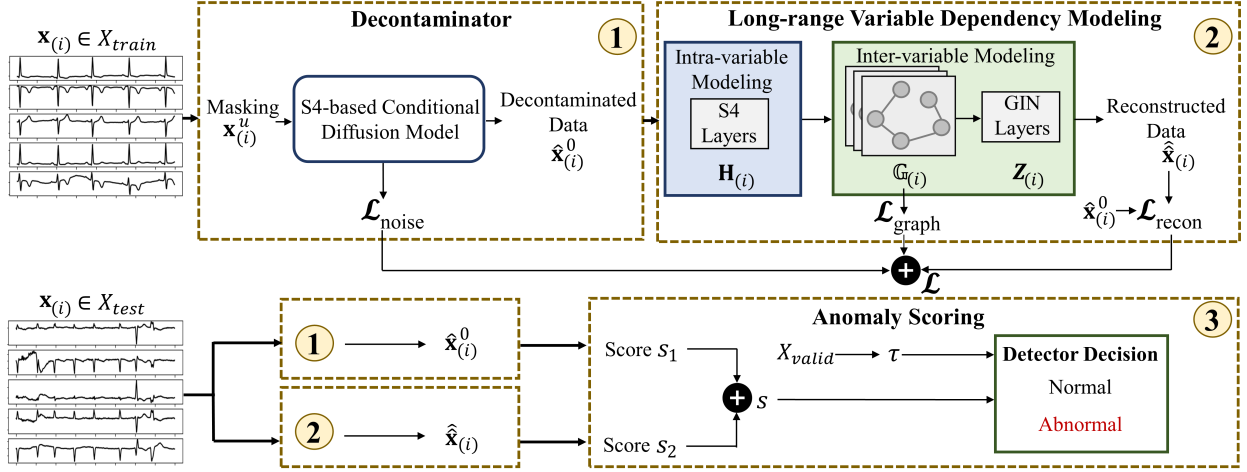


Figure 1: The overall framework of TSAD-C consists of three core modules: the Decontaminator integrates masking strategies and an S4-based diffusion model, the Long-Range Variable Dependency Modeling module incorporates Intra- and Inter-variable Modeling components; and the Anomaly Scoring module leverages insights from the preceding modules to detect anomalies.

that $\mathbf{x}_{(i)}^t$ is sampled from a normal distribution with mean $\mu_{(i)}^t = \sqrt{1 - \beta_t} \mathbf{x}_{(i)}^{t-1}$ and variance $\sigma_{(i)}^t = \beta_t \mathbf{I}$. \mathbf{I} is the identity matrix, $\beta_t \in (0, 1)$ is a variance scheduler that controls the quantity of noise added at the t th diffusion step. In our implementation, we increase β_t linearly from 10^{-4} to 0.02. By setting $\alpha_t = 1 - \beta_t$, $\bar{\alpha}_t = \prod_{j=1}^t \alpha_j$, the diffusion process allows to immediately transform $\mathbf{x}_{(i)}^0$ to a noisy $\mathbf{x}_{(i)}^t$ according to β_t in a closed form as $\mathbf{x}_{(i)}^t = \sqrt{\bar{\alpha}_t} \mathbf{x}_{(i)}^0 + \sqrt{1 - \bar{\alpha}_t} \epsilon_t$ where the noise $\epsilon_t \sim \mathcal{N}(0, \mathbf{I})$, $\epsilon_t \in \mathbb{R}^{K \times L}$. We add noise to both masked and non-masked portions of $\mathbf{x}_{(i)}^0$. As the diffusion step increases, $\mathbf{x}_{(i)}^0$ gradually loses its distinguishable features and approaches a Gaussian distribution; hence, both anomalous and normal patterns appear indistinguishable.

The reverse process is parameterized by θ as:

$$q_{\theta}(\mathbf{x}_{(i)}^0, \dots, \mathbf{x}_{(i)}^{T-1} | \mathbf{x}_{(i)}^T) = \prod_{t=1}^T q_{\theta}(\mathbf{x}_{(i)}^{t-1} | \mathbf{x}_{(i)}^t), \quad (2)$$

where each $q_{\theta}(\mathbf{x}_{(i)}^{t-1} | \mathbf{x}_{(i)}^t) := \mathcal{N}(\mathbf{x}_{(i)}^{t-1}; \mu_{\theta}(\mathbf{x}_{(i)}^t, t, c), \sigma_{\theta}(\mathbf{x}_{(i)}^t, t, c)^2 \mathbf{I})$. μ_{θ} and σ_{θ} are parameterized as:

$$\begin{aligned} \mu_{\theta}(\mathbf{x}_{(i)}^t, t, c) &= \frac{1}{\sqrt{\bar{\alpha}_t}} \left(\mathbf{x}_{(i)}^t - \frac{\beta_t}{\sqrt{1 - \bar{\alpha}_t}} \epsilon_{\theta}(\mathbf{x}_{(i)}^t, t, c) \right), \\ \sigma_{\theta}(\mathbf{x}_{(i)}^t, t, c) &= \sqrt{\bar{\beta}_t}, \end{aligned} \quad (3)$$

where $\bar{\beta}_t = \frac{1 - \bar{\alpha}_{t-1}}{1 - \bar{\alpha}_t} \beta_t$ and $\bar{\beta}_1 = \beta_1$. ϵ_{θ} is a noise estimator, which takes $\mathbf{x}_{(i)}^t$, the diffusion step t and a conditional factor c as the inputs and aims to predict the noise from $\mathbf{x}_{(i)}^t$. c is a concatenation of the non-masked segments in $\mathbf{x}_{(i)}^u$ and the positional information of the masked parts provided by \mathbf{v} . This extra information facilitates our reverse process to distinguish the zero portions of non-masked and masked parts.

Note that ϵ_{θ} plays a key role in our reverse process. Since capturing long-range intra-variable dependencies is crucial,

we propose to build ϵ_{θ} based on S4 (Gu et al. 2022) - a recent deep sequence model with the concept of a state space model (SSM). A continuous-time SSM maps $\mathbf{x}_{(i)}^t$ to a high dimensional state $h_{(i)}^t$ before projecting it to the output $\mathbf{y}_{(i)}^t$. This transition can be defined as:

$$\tilde{h}_{(i)}^t = A h_{(i)}^t + B \mathbf{x}_{(i)}^t \text{ and } \mathbf{y}_{(i)}^t = C h_{(i)}^t + D \mathbf{x}_{(i)}^t, \quad (4)$$

where A, B, C, D are transition matrices learned by gradient descent. However, S4 shows that a discrete-time SSM can be represented as a convolution operation by:

$$\bar{O} := (\bar{C}\bar{B}, \bar{C}\bar{A}\bar{B}, \dots, \bar{C}\bar{A}^{L-1}\bar{B}), \mathbf{y}_{(i)} = \bar{O} * \mathbf{x}_{(i)}, \quad (5)$$

where $\bar{A}, \bar{B}, \bar{C}$ are the discretized matrices, $\bar{C}\bar{A}^{L-1}$ denotes the multiplication of discretized matrices at $L - 1$, and \bar{O} is a SSM convolution kernel. D is omitted in Equation (5) as $D\mathbf{x}_{(i)}^t$ can be viewed as a skip connection. Essentially, S4 parameterizes A as a diagonal plus low rank matrix, enabling fast computation of \bar{O} . It also includes the HiPPO matrices (Gu et al. 2020) capable of capturing long-term intra-variable dependencies. We employ two S4 layers, one after the addition of the embeddings related to $\mathbf{x}_{(i)}^u$ and another layer after including c in the residual blocks (see Figure 2).

To have a simpler and more streamlined reverse process during the training of ϵ_{θ} , we suggest minimizing the noise error on the masked parts shown in Equation (6). Note that the masked parts only consist of noise without any actual data patterns, unlike the non-masked parts containing both noise and the actual data patterns. Hence, deriving noise estimated from the masked data is a more straightforward task and can be accomplished using less intricate networks. This approach also speeds up data preparation for subsequent modules. In our experiments, we have compared two optimization strategies: minimizing $\mathcal{L}_{\text{noise}}$ on the masked portions versus minimizing $\mathcal{L}_{\text{noise}}$ on the entire observations as done by prior diffusion studies (Alcaraz and Strothoff

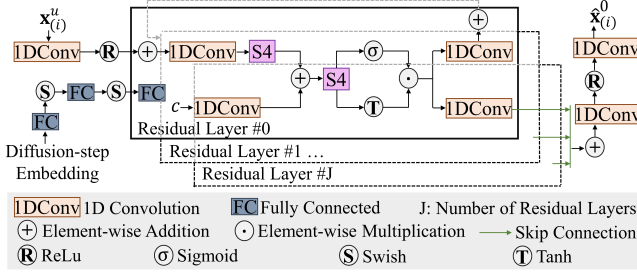


Figure 2: The architecture of the Decontaminator includes two S4 layers in every residual block to ensure that long-range intra-variable dependencies are effectively captured.

2022; Chen et al. 2024). It shows that the former approach yields superior performance, simplicity and applicability.

$$\mathcal{L}_{\text{noise}} = \|\epsilon_t \odot (1 - \mathbf{v}) - \hat{\epsilon}_t \odot (1 - \mathbf{v})\|^2, \quad (6)$$

where $\hat{\epsilon}_t$ is the predicted noise obtained from $\epsilon_\theta(\mathbf{x}_{(i)}^t, t, c)$.

We then obtain the decontaminated data in the training as:

$$\hat{\mathbf{x}}_{(i)}^0 = \frac{1}{\sqrt{\alpha_T}} \left(\mathbf{x}_{(i)}^T - \sqrt{1 - \alpha_T} \hat{\epsilon}_T \right). \quad (7)$$

Note that approximating $\hat{\mathbf{x}}_{(i)}^0$ by a *single* step (immediately at the T th step) enables a faster reverse speed as $\hat{\mathbf{x}}_{(i)}^0$ serves as the input for the second module during training. Meanwhile, during testing, we perform a complete sampling step from T to 1 based on Equations (2) and (3) to obtain $\hat{\mathbf{x}}_{(i)}^0$.

2.2. Long-range Variable Dependency Modeling

This module builds a time-then-graph framework, motivated in **Section 1-Paragraph 5**, by incorporating two components: Intra-variable Modeling and Inter-variable Modeling.

Intra-variable Modeling. We propose to leverage multiple back-to-back S4 layers to capture long-range intra-variable dependencies. Specifically, we use $\hat{\mathbf{x}}_{(i)}^0 \in \mathbb{R}^{K \times L}$ as the input and project it onto an embedding space, called $\mathbf{H}_{(i)} \in \mathbb{R}^{K \times \Gamma \times U}$, where Γ and U are hyperparameters defining the S4 embedding dimension. To maintain a sense of the number of timestamps present in $\mathbf{x}_{(i)}$, we set Γ to L , corresponding to the input length. This allows us to model long-term intra-variable dependencies within each variable. $\mathbf{H}_{(i)}$ is then used in the graph learning phase to model inter-variable dependencies. Prior studies have shown the superior performance of graph learning when using the temporal embedding rather than the original data (Tang et al. 2023).

Inter-variable Modeling. We represent $\mathbf{H}_{(i)}$ as a set of graphs $\mathbb{G}_{(i)} = \{\mathcal{G}_{(i)}^m\}_{m=1}^d$, where $d = \frac{\Gamma}{g}$ and g is the pre-defined length of the short and non-overlapping time windows within the i th observation. Since each observation can encompass thousands of timestamps, constructing a graph for every time step becomes inefficient and computationally demanding. Hence, we create a graph over a defined time window, which aids in information aggregation. This strategy not only leads to a graph with reduced noise but also facilitates faster computations (Gao and Ribeiro 2022).

We define $\mathcal{G}_{(i)}^m = \{\mathbf{E}_{(i)}^m, \mathcal{A}_{(i)}^m\}$. $\mathbf{E}_{(i)}^m \in \mathbb{R}^{K \times U}$ denotes the embedding derived by averaging the elements of $\mathbf{H}_{(i)}$ along its second dimension. $\mathcal{A}_{(i)}^m \in \mathbb{R}^{K \times K}$ is the adjacency matrix. Each row and column in $\mathcal{A}_{(i)}^m$ correspond to a node (variable). The non-zero value indicates that there exists an edge connecting the two nodes. We then employ a self-attention paradigm (Tang et al. 2023) in which attention weights are assigned to the edges’ weights, represented as:

$$\begin{aligned} \mathbf{Q} &= \mathbf{E}_{(i)}^m \mathbf{W}^{\mathbf{Q}}, \mathbf{R} = \mathbf{E}_{(i)}^m \mathbf{W}^{\mathbf{R}}, \\ \mathcal{A}_{(i)}^m &= \text{softmax}\left(\frac{\mathbf{Q}\mathbf{R}^{\top}}{\sqrt{D}}\right), \end{aligned} \quad (8)$$

where $\mathbf{W}^{\mathbf{Q}}, \mathbf{W}^{\mathbf{R}} \in \mathbb{R}^{U \times U}$ are the learnable weights that project $\mathbf{E}_{(i)}^m$ to the query \mathbf{Q} and the key \mathbf{R} , respectively.

To help guiding the graph learning process, we also include a pre-defined adjacency matrix, called $\mathcal{A}_{(i)}^m$, based δ -nearest neighbors. Its edge values are computed by the cosine similarity between the nodes’ embeddings in $\mathbf{E}_{(i)}^m$. We keep the top δ edges that have the highest values for each node to avoid overly connected graphs. In our experiments, $\delta = 3$. Hence, the final $\mathcal{A}_{(i)}^m = \zeta \mathcal{A}_{(i)}^m + (1 - \zeta) \mathcal{A}_{(i)}^m$, where the hyperparameter $\zeta \in [0, 1)$ balances the two components.

It is important to regularize the graph to ensure desired graph properties such as smoothness (the features should change smoothly between neighboring nodes), sparsity (avoiding an overly connected graph) and connectivity (avoiding a disconnected graph) (Zhu et al. 2022). Hence, we include three constraints in the regularization loss as:

$$\begin{aligned} \mathcal{L}_{\text{graph}} &= \frac{1}{d} \sum_{m=1}^d \xi_1 \mathcal{L}_{\text{smooth}}(\mathbf{E}_{(i)}^m, \mathcal{A}_{(i)}^m) + \\ &\xi_2 \mathcal{L}_{\text{sparse}}(\mathcal{A}_{(i)}^m) + \xi_3 \mathcal{L}_{\text{connect}}(\mathcal{A}_{(i)}^m), \end{aligned} \quad (9)$$

where $\mathcal{L}_{\text{smooth}} = \frac{1}{K^2} \text{tr}(\mathbf{E}_{(i)}^m \mathbf{M}_{\text{Lap}} \mathbf{E}_{(i)}^m)$, $\mathbf{M}_{\text{Lap}} = \mathbf{M}_{\text{degree}} - \mathcal{A}_{(i)}^m$ is the Laplacian matrix, $\mathbf{M}_{\text{degree}}$ is the degree matrix of $\mathcal{A}_{(i)}^m$, and $\text{tr}(\cdot)$ denotes the trace. $\mathcal{L}_{\text{sparse}} = \frac{1}{K^2} \|\mathcal{A}_{(i)}^m\|_F^2$ and $\|\cdot\|_F$ is the Frobenius norm. $\mathcal{L}_{\text{connect}} = -\frac{1}{K} \mathbf{1}^{\top} \log(\mathcal{A}_{(i)}^m \cdot \mathbf{1})$, and $\mathbf{1} \in \mathbb{R}^{K \times 1}$ is a matrix of ones. ξ_1, ξ_2 and ξ_3 are hyperparameters defined to balance the terms in $\mathcal{L}_{\text{graph}}$.

We then leverage a graph isomorphism network (GIN), which shows a strong representational power (Xu et al. 2019) to capture inter-variable dependencies between nodes in $\mathcal{G}_{(i)}^m$. The embedding of nodes in $\mathcal{G}_{(i)}^m$ is represented as $\mathbf{z}_{(i)}^m := \text{GIN}(\mathbf{E}_{(i)}^m, \mathcal{A}_{(i)}^m)$, $\mathbf{z}_{(i)}^m \in \mathbb{R}^{K \times g \times U}$. We concatenate the node embeddings of all graphs within $\mathbb{G}_{(i)}$ as $\mathbf{Z}_{(i)} = \text{concat}(\mathbf{z}_{(i)}^1, \dots, \mathbf{z}_{(i)}^d)$. Finally, a linear layer is added to obtain reconstructed data $\hat{\mathbf{x}}_{(i)} := \text{Linear}(\mathbf{Z}_{(i)})$, $\hat{\mathbf{x}}_{(i)} \in \mathbb{R}^{K \times L}$. Thus, the reconstruction loss is denoted as:

$$\mathcal{L}_{\text{recon}} = \|\hat{\mathbf{x}}_{(i)}^0 - \hat{\mathbf{x}}_{(i)}\|^2. \quad (10)$$

The final loss in the training phase is defined as :

$$\mathcal{L} = \mathcal{L}_{\text{noise}} + \mathcal{L}_{\text{graph}} + \mathcal{L}_{\text{recon}}. \quad (11)$$

2.3. Anomaly Scoring

In the test phase, we compute an anomaly score based the root mean square error (RMSE) for each $\mathbf{x}_{(i)}$. Specifically, we project $\mathbf{x}_{(i)}$ to the Decontaminator where masking strategies and the complete sampling step from T to 1 are applied to obtain $\hat{\mathbf{x}}_{(i)}^0$. If $\mathbf{x}_{(i)}$ is an anomaly, the masked portions are expected to be inaccurately sampled. At the same time, instead of using $\hat{\mathbf{x}}_{(i)}^0$ as the input for the second module as done during training, $\mathbf{x}_{(i)}$ is directly used to obtain $\hat{\hat{\mathbf{x}}}_{(i)}$ in the test phase. The assumption is that if $\mathbf{x}_{(i)}$ is an anomaly, the second module with the goal of achieving the flawless reconstruction of normal patterns would be unable to reconstruct it. The final score s for each $\mathbf{x}_{(i)}$ is computed as:

$$\begin{aligned} s_1 &= \left(\frac{1}{L} \sum_{l=1}^L \sum_{k=1}^K \left((\hat{\mathbf{x}}_{(i)}^0 - \mathbf{x}_{(i)}) \odot (1 - \mathbf{v}) \right)^2 \right)^{0.5}, \\ s_2 &= \left(\frac{1}{L} \sum_{l=1}^L \sum_{k=1}^K \left(\hat{\hat{\mathbf{x}}}_{(i)} - \mathbf{x}_{(i)} \right)^2 \right)^{0.5}, \\ s &= \lambda_1 s_1 + \lambda_2 s_2, \end{aligned} \quad (12)$$

where s_1 and s_2 are, respectively, the RMSE scores obtained from the first and second modules. λ_1 and λ_2 are hyperparameters defined to ensure that anomaly scores from both modules fall within a similar numeric range. For a fair comparison, they are fixed across all experiments and datasets.

We conduct a decision threshold search on the *unlabeled* X_{valid} , deviating from the TSAD practice where the threshold is selected on a *labeled* set (Carmona et al. 2022; Chen et al. 2022). This approach is impractical for unsupervised applications where labeled data is unavailable. This may also lead to overfitting when labeled data is not sufficient to represent the distribution of anomalies, a common challenge in TSAD. In our case, we determine the threshold τ by a quantile approach (Kuan et al. 2017) applied to the anomaly scores obtained from the unlabeled X_{valid} . Specifically, we select a quantile based on a rough estimation of the percentage of normal data in X_{valid} , as provided by the dataset provider. For instance, if about 20% of the data is contaminated, we set the quantile to 80%. In the test phase, observations with s above τ are detected as anomalies. Note that there is no overlap between X_{train} , X_{valid} , and X_{test} . Overall, our threshold finding approach eliminates the need for labeled data, while mitigating the risk of overfitting by relying on distributional characteristics rather than specific samples.

3. Experiments

3.1. Experimental Settings

In this section, we introduce the datasets, baselines, implementation details, and performance evaluation metrics in our study.

Datasets. Numerous TSAD methods have relied on benchmark datasets such as Yahoo, NASA, SWaT, WADI, SMAP, and MSL. However, these datasets are unreliable due to (i) mislabeled ground truth, (ii) triviality, (iii) unrealistic anomaly density and (iv) run-to-failure bias, which prompts algorithms to simply detect the last points as anomalies (Wu and Keogh 2021; Wagner et al. 2023). This renders them

Dataset	$X_{\text{train}} (\eta)$	$X_{\text{valid}} (\eta)$	$X_{\text{test}} (\eta)$	f_s	K	L
SMD	1624 (10.3%)	276 (7.97%)	416 (33.8%)	$\frac{1}{60}$	38	600
ICBEB	910 (20.0%)	82 (20.7%)	222 (59.9%)	100	12	6,000
DODH	2515 (19.8%)	320 (21.8%)	310 (51.6%)	250	16	7,500
TUSZ	5275 (17.0%)	1055 (20.0%)	1581 (40.0%)	200	19	12,000

Table 1: The numbers of observations are shown in X_{train} , X_{valid} and X_{test} of each dataset, with the anomaly ratio η in parentheses. f_s is the sampling rate (in Hertz), K is the number of variables, and L is the length of an observation.

unsuitable for evaluating TSAD methods. Aware of these issues, we carefully select four reliable datasets from various domains, recorded using diverse sensor systems, each varying in the number and types of sensors. These include **SMD** (Su et al. 2019) - an industrial dataset consisting of five weeks of data from 28 server machines. While not perfect, SMD is of much higher quality than other criticized datasets (Wagner et al. 2023). To ensure a rigorous and robust evaluation of TSAD algorithms on SMD, we perform interval-level TSAD as defined in **Section 2** - Paragraph 1, aligning with recent standards in TSAD (Lai et al. 2024). This avoids point-adjustment bias - a common issue in TSAD (Kim et al. 2022). Moreover, we model all 28 machines together instead of individually (Su et al. 2019).

Three additional datasets are **ICBEB** (Liu et al. 2018), **DODH** (Guillot et al. 2020), and **TUSZ** (Shah et al. 2018). They are well-established yet challenging datasets from the biomedical domain and have not received criticisms (i)-(iv). To minimize human labeling errors, they are annotated by a consensus of 3-5 experts, considering factors such as patient history, symptoms, diagnostic tests, and treatment outcomes. They often exhibit long-range intra-variable dependencies, reflecting phenomena like physiological states or disease progression, which oversimplified models cannot capture complex time-series dynamics. Importantly, they reflect real-world scenarios with diverse anomaly types, while other datasets such as SMD contain only one anomaly type.

Specifically, ICBEB is an electrocardiogram database, consisting of normal heart rhythms and five anomaly types: atrial fibrillation, first-degree atrioventricular, right bundle branch, ventricular contraction, and ST-segment elevation. DODH is a sleep database, with N3 (the deepest sleep stage) as normal and two anomaly types: Awake and REM. TUSZ is an electroencephalogram database, with normal resting-state brain activities and two anomaly types: focal seizures and generalized seizures. Details of each dataset are shown in Table 1. Note that we include 10-20% anomalies of all types in X_{train} to contaminate normal data during training, increasing the challenge for algorithms to detect all anomaly types in the test phase.

Baselines. We compare TSAD-C against 12 SOTA unsupervised methods from the TSAD literature, ranging from autoencoders, self-supervised, transformers to diffusion approaches. For a fair comparison, we do not include methods that require transfer learning with any additional datasets. We categorize all methods into three groups based on their

Method	SMD			ICBEB			DODH			TUSZ			Average	
	F1	Rec	APR	F1	Rec	APR	F1	Rec	APR	F1	Rec	APR	F1	
Intra-	USAD	0.261	0.227	0.398	0.579	0.485	0.705	0.355	0.419	0.514	0.450	0.393	0.581	0.411
	LSTM-AE	0.332	0.411	0.445	0.609	0.651	0.752	0.534	0.706	0.643	0.471	0.424	0.592	0.486
	S4-AE	0.313	0.305	0.432	0.664	0.735	0.749	0.625	0.821	0.713	0.527	0.576	0.615	0.532
	DCdetector	0.318	0.276	0.448	0.626	0.598	0.718	0.442	0.550	0.576	0.485	0.447	0.600	0.468
Inter-	GAE	0.241	0.191	0.395	0.575	0.454	0.746	0.480	0.613	0.604	0.508	0.476	0.625	0.451
	GDN	0.301	0.283	0.423	0.586	0.515	0.741	0.524	0.687	0.636	0.456	0.398	0.585	0.467
	EEG-CGS	0.295	0.291	0.415	0.561	0.470	0.740	0.502	0.650	0.620	0.516	0.490	0.619	0.469
Both-	InterFusion	0.383	0.504	0.490	0.649	0.651	0.753	0.418	0.512	0.559	0.532	0.520	0.628	0.496
	GRU-GNN	0.329	0.383	0.440	0.647	0.689	0.742	0.587	0.806	0.684	0.506	0.474	0.613	0.517
	DVGRN	0.323	0.305	0.442	0.615	0.575	0.744	0.480	0.612	0.604	0.397	0.322	0.554	0.479
	GraphS4mer	0.405	0.567	0.514	0.638	0.667	0.738	0.565	0.762	0.667	0.524	0.511	0.621	0.533
	IMDiffusion	0.426	0.603	0.533	0.611	0.553	0.750	0.544	0.725	0.651	0.381	0.452	0.532	0.491
	TSAD-C	0.479	0.801	0.604	0.707	0.841	0.773	0.652	0.843	0.728	0.545	0.830	0.652	0.596

Table 2: Comparison between existing methods and ours. The best and second-best scores are denoted in bold and underlined.

ability to capture either Intra-, Inter- or Both-variable dependencies. Specifically, Intra- methods include USAD (Audibert et al. 2020), LSTM-AE (Wei et al. 2023), S4-AE (Gu et al. 2022) and DCdetector (Yang et al. 2023). Inter- methods are GAE (Du et al. 2022), GDN (Deng and Hooi 2021), and EEG-CGS (Ho and Armanfard 2023). Methods addressing Both- include InterFusion (Li et al. 2021), DVGRN (Chen et al. 2022), GRU-GNN and GraphS4mer (Tang et al. 2023), IMDiffusion (Chen et al. 2024) and our method.

Evaluation Metrics. We employ F1-score (F1), Recall (Rec), and Area Under the Precision-Recall Curve (APR) to comprehensively assess the performance of each method.

3.2. Comparison with State-of-the-art

The performances of all methods are presented in Table 2, where TSAD-C uses RandBM. It shows that TSAD-C surpasses all existing studies and achieves an average improvement of 6.3% in F1 compared to the second-best method. TSAD-C also obtains a significant improvement in Rec (the ability to correctly detect most of anomalies). This improvement is crucial when dealing with contaminated data, where existing methods failed to detect the types of anomalies similar to those encountered during training due to their assumption of clean training data, leading to misdetection of such anomalies. We also observe that existing methods handling Both- generally outperform those addressing only one dependency type, supporting our assumption that both types of dependencies are crucial. Moreover, methods handling long-range Intra- (e.g., S4-AE) outperform those concentrating solely on Inter-. This suggests that while inter-variable dependencies are also important, they often represent immediate relationships between variables that can be captured over shorter temporal windows, which might miss the broader temporal context necessary to detect anomalies effectively.

3.3. Resilience to Contamination Levels

This section verifies TSAD-C’s performance through two additional experiments on ICBEB: (1) varying the number of anomaly types and (2) varying the anomaly ratio η in X_{train}

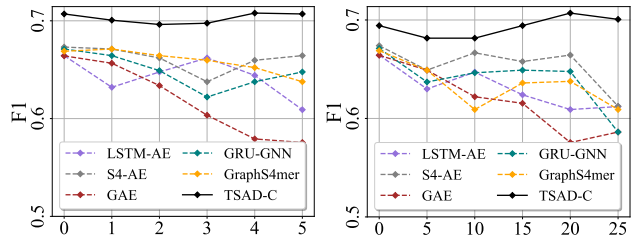


Figure 3: (Left) F1 score versus the number of anomaly types κ . (Right) F1 score versus the anomaly ratio η .

and X_{valid} . We also select five methods, each achieving high performance within its category, for comparison.

Variability on The Anomaly Types. We assess the performance of TSAD-C in detecting five anomaly types available in X_{test} while not all types are present in X_{train} and X_{valid} . We introduce κ as the number of anomaly types – e.g., $\kappa = 2$ signifies two anomaly types present in X_{train} and X_{valid} . Note that η remains constant. Figure 3 (Left) shows that the performance of unsupervised methods diminishes as κ increases since they all assume the given input data as pure normal data, hence are incapable of handling contaminated data. These methods face more difficulties when the input data impurity increases. Remarkably, TSAD-C consistently attains the highest F1, irrespective of changes in κ . This underlines our method’s denoising prowess as it remains effective regardless of the diversity in available anomaly types.

Variability on The Anomaly Ratio. We investigate the robustness of TSAD-C by varying η . Note that all anomaly types ($\kappa = 5$) are present within each subset of the dataset for this experiment. Figure 3 (Right) shows the consistent performance of TSAD-C across different anomaly ratios, demonstrating the Decontaminator’s effectiveness in TSAD-C. Meanwhile, the performance of other unsupervised methods tends to decline as normal data impurity increases.

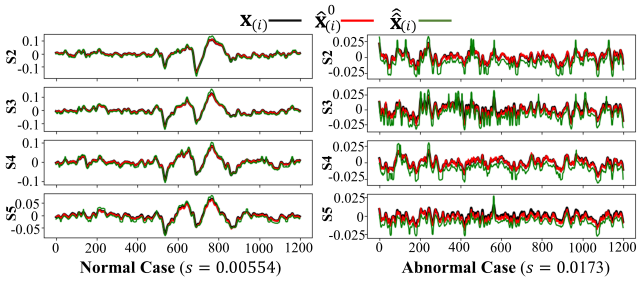


Figure 4: Comparison between normal and abnormal cases for the masked segment in DODH (S: Sensor). The masked strategy used is BoM. Each case includes $\mathbf{x}_{(i)}$, $\hat{\mathbf{x}}_{(i)}^0$ and $\hat{\mathbf{x}}_{(i)}$.

3.4. Visualization of Normal Approximation

Figure 4 shows a visualization comparing the ground truth $\mathbf{x}_{(i)}$, decontaminated data $\hat{\mathbf{x}}_{(i)}^0$, and reconstructed data $\hat{\mathbf{x}}_{(i)}$ of a masked segment of normal and abnormal samples in DODH. The segment of $\mathbf{x}_{(i)}$ is masked to zeros using BoM, before being processed by the Decontaminator. It is shown that $\hat{\mathbf{x}}_{(i)}^0$ and $\hat{\mathbf{x}}_{(i)}$ fit $\mathbf{x}_{(i)}$ very well in the normal case, leading to a lower s . Meanwhile, there are significant fluctuations of $\hat{\mathbf{x}}_{(i)}^0$ and $\hat{\mathbf{x}}_{(i)}$ compared to $\mathbf{x}_{(i)}$ in the abnormal case, resulting in a much higher s . This shows TSAD-C’s effectiveness in distinguishing anomalies from normal data.

3.5. Ablation Study

Certainly, handling contaminated data requires the indispensable inclusion of Module (1) - Decontaminator. Excluding it would align the TSAD-C’s detection results with those of other unsupervised methods. Hence, we conduct ablation studies specifically focusing on Module (2) - Long-range Variable Dependency Modeling, and Module (3) - Anomaly Scoring, as shown in Table 3. RandBM is used in all experiments. The sign “-” denotes the exclusion of a component.

Module (2). The results are shown in the first and second rows, where Intra and Inter, respectively, denote the Intra-variable Modeling, and Inter-variable Modeling. Note that for this experiment, the anomaly score s_2 is computed by the non-removed block of Module (2), i.e., for the first and second rows, s_2 is determined by Inter and Intra, respectively. The results highlight the superior performance achieved by capturing long-range intra-variable dependencies, showing that while Inter is also an important component, having Intra is often prioritized due to the nature of time-series data.

Module (3). In this study, all components of Modules (1) and (2) are available during training, whereas we exclude either s_1 or s_2 , respectively, obtained from Module (1) or Module (2) during testing. The results, shown in the third and fourth rows, indicate that by removing either s_1 or s_2 , we observe a small drop in performance. This is due to the fact that in the test phase, we still perform data decontamination using the Decontaminator trained during training. Such data decontamination during testing resembles a case where one performs the unsupervised anomaly detection of the clean test data. This experiment can be considered as a

TSAD-C	Metric	ICBEB	DODH	TUSZ	
Module (2)	- Intra	F1	0.651	0.565	0.499
		{Rec; APR}	{0.735; 0.738}	{0.637; 0.667}	{0.655; 0.598}
-	- Inter	F1	0.686	0.622	0.535
		{Rec; APR}	{0.803; 0.759}	{0.762; 0.705}	{0.789; 0.639}
Module (3)	- s_1	F1	0.706	0.637	0.517
		{Rec; APR}	{0.856; 0.771}	{0.80; 0.716}	{0.745; 0.622}
	- s_2	F1	0.699	0.627	0.518
		{Rec; APR}	{0.818; 0.768}	{0.787; 0.709}	{0.712; 0.617}
All	F1	0.707	0.652	0.545	
	{Rec; APR}	{0.841; 0.773}	{0.843; 0.728}	{0.830; 0.652}	

Table 3: Performance of individual components in TSAD-C.

Method	Metric	ICBEB	DODH	TUSZ
RandM	F1	0.694	0.647	0.520
		{Rec; APR}	{0.825; 0.764}	{0.837; 0.724}
RandBM	F1	0.707	0.652	0.545
		{Rec; APR}	{0.841; 0.773}	{0.843; 0.728}
BoM	F1	0.669	0.623	0.531
		{Rec; APR}	{0.795; 0.747}	{0.806; 0.707}

Table 4: Comparison between different masking strategies.

demonstration of the Decontaminator’s effectiveness.

Importantly, integrating all components together both in training and test phases (aka **All**) yields the best performance across all datasets, as shown in the the last row, showcasing the synergistic complementarity of each component in enhancing the model’s ability to detect anomalies.

3.6. Effect of Masking Strategy

This section evaluates the performance of TSAD-C with various masking strategies. Note that we maintain a fixed value for r , which is used to control the masking ratio, to avoid hyperparameter fine-tuning. The consistency of better performance of TSAD-C even with a fixed r , irrespective of changes in the anomaly ratio η , is demonstrated in Figure 3 (Right). Table 4 shows that the performance of TSAD-C remains largely consistent across RandM, RandBM, and BoM (with a fixed r). Despite the consistency, RandBM showcases the most optimal performance. This can be attributed to introducing randomness into the masked time windows, which increases the level of robustness and adaptability to diverse patterns in the data. This is crucial for real-world applications where anomalies can manifest in diverse ways across sensors. RandBM emulates this diversity, enabling the model to learn and detect sensor-specific anomalies more effectively, thus boosting its overall performance.

4. Conclusion

This paper introduces TSAD-C, the first method trained on contaminated data to detect all types of anomalies in multivariate time series. TSAD-C comprises the Decontaminator, aimed at removing the potentially anomalous patterns during training. Given decontaminated data prepared swiftly by the Decontaminator, we propose the Long-range Variable De-

pendency Modeling module to capture long-range intra- and inter-variable dependencies and provide an approximation of purified data. An Anomaly Scoring module is achieved by integrating the capability of the first two modules. We demonstrate the superior performance of TSAD-C on four reliable and diverse datasets compared to existing methods.

Acknowledgments

The authors would like to acknowledge the financial support of the Natural Sciences, Engineering Research Council of Canada (NSERC), Fonds de recherche du Quebec, and the Department of Electrical and Computer Engineering at McGill University. The authors also wish to thank Calcul Quebec and Compute Canada for providing the necessary computational resources to conduct our experiments.

References

- Alcaraz, J. M. L.; and Strodthoff, N. 2022. Diffusion-based time series imputation and forecasting with structured state space models. *Transactions on Machine Learning Research*.
- Audibert, J.; Michiardi, P.; Guyard, F.; Marti, S.; and Zuluaga, M. A. 2020. Usad: Unsupervised anomaly detection on multivariate time series. In *Proceedings of the 26th ACM SIGKDD international conference on knowledge discovery & data mining*, 3395–3404.
- Carmona, C. U.; Aubet, F.-X.; Flunkert, V.; and Gasthaus, J. 2022. Neural contextual anomaly detection for time series. In *International Joint Conference on Artificial Intelligence*.
- Chen, W.; Tian, L.; Chen, B.; Dai, L.; Duan, Z.; and Zhou, M. 2022. Deep variational graph convolutional recurrent network for multivariate time series anomaly detection. In *International Conference on Machine Learning*, 3621–3633. PMLR.
- Chen, Y.; Zhang, C.; Ma, M.; Liu, Y.; Ding, R.; Li, B.; He, S.; Rajmohan, S.; Lin, Q.; and Zhang, D. 2024. Imdiffusion: Imputed diffusion models for multivariate time series anomaly detection. *Proceedings of the VLDB Endowment*.
- Croitoru, F.-A.; Hondru, V.; Ionescu, R. T.; and Shah, M. 2023. Diffusion models in vision: A survey. *IEEE Transactions on Pattern Analysis and Machine Intelligence*, 45(9): 10850–10869.
- Deng, A.; and Hooi, B. 2021. Graph neural network-based anomaly detection in multivariate time series. In *Proceedings of the AAAI conference on artificial intelligence*, 4027–4035.
- Du, X.; Yu, J.; Chu, Z.; Jin, L.; and Chen, J. 2022. Graph autoencoder-based unsupervised outlier detection. *Information Sciences*, 608: 532–550.
- Gao, J.; and Ribeiro, B. 2022. On the equivalence between temporal and static equivariant graph representations. In *International Conference on Machine Learning*, 7052–7076. PMLR.
- Gu, A.; Dao, T.; Ermon, S.; Rudra, A.; and Ré, C. 2020. Hippo: Recurrent memory with optimal polynomial projections. *Advances in neural information processing systems*, 33: 1474–1487.
- Gu, A.; Goel; Karan; and Ré, C. 2022. Efficiently modeling long sequences with structured state spaces. In *International Conference on Learning Representations*.
- Guillot, A.; Sauvet, F.; During, E. H.; and Thorey, V. 2020. Dream open datasets: Multi-scored sleep datasets to compare human and automated sleep staging. *IEEE transactions on neural systems and rehabilitation engineering*, 28(9): 1955–1965.
- Ho, T. K. K.; and Armanfard, N. 2023. Self-Supervised Learning for Anomalous Channel Detection in EEG Graphs: Application to Seizure Analysis. In *Proceedings of the AAAI Conference on Artificial Intelligence*, volume 37, 7866–7874.
- Ho, T. K. K.; Karami, A.; and Armanfard, N. 2023. Graph-based Time-Series Anomaly Detection: A Survey. *arXiv preprint arXiv:2302.00058*.
- Jiang, X.; Liu, J.; Wang, J.; Nie, Q.; Wu, K.; Liu, Y.; Wang, C.; and Zheng, F. 2022. Softpatch: Unsupervised anomaly detection with noisy data. *Advances in Neural Information Processing Systems*, 35: 15433–15445.
- Katharopoulos, A.; Vyas, A.; Pappas, N.; and Fleuret, F. 2020. Transformers are rns: Fast autoregressive transformers with linear attention. In *International Conference on Machine Learning*, 5156–5165. PMLR.
- Kim, S.; Choi, K.; Choi, H.-S.; Lee, B.; and Yoon, S. 2022. Towards a rigorous evaluation of time-series anomaly detection. In *Proceedings of the AAAI Conference on Artificial Intelligence*, 7194–7201.
- Kuan, C.-M.; Michalopoulos; Christos; and Xiao, Z. 2017. Quantile regression on quantile ranges—A threshold approach. *Journal of Time Series Analysis*, 38(1): 99–119.
- Lai, T.; Ho; Khanh, T. K.; and Armanfard, N. 2024. Open-Set Multivariate Time-Series Anomaly Detection. In *European Conference on Artificial Intelligence*.
- Li, Z.; Zhao, Y.; Han, J.; Su, Y.; Jiao, R.; Wen, X.; and Pei, D. 2021. Multivariate time series anomaly detection and interpretation using hierarchical inter-metric and temporal embedding. In *Proceedings of the 27th ACM SIGKDD conference on knowledge discovery & data mining*, 3220–3230.
- Lim, S. H.; Erichson, N. B.; Hodgkinson, L.; and Mahoney, M. W. 2021. Noisy recurrent neural networks. *Advances in Neural Information Processing Systems*, 34: 5124–5137.
- Liu, F.; Liu, C.; Zhao, L.; Zhang, X.; Wu, X.; Xu, X.; Liu, Y.; Ma, C.; Wei, S.; He, Z.; et al. 2018. An open access database for evaluating the algorithms of electrocardiogram rhythm and morphology abnormality detection. *Journal of Medical Imaging and Health Informatics*, 8(7): 1368–1373.
- Pradhan, A.; He, J.; and Jiang, N. 2022. Hand gesture recognition and biometric authentication using a multi-day dataset. In *Intelligent Robotics and Applications: 15th International Conference, ICIRA 2022, Harbin, China, August 1–3, 2022, Proceedings, Part IV*, 375–385. Springer.
- Schmidl, S.; Wenig, P.; and Papenbrock, T. 2022. Anomaly detection in time series: a comprehensive evaluation. *Proceedings of the VLDB Endowment*, 15(9): 1779–1797.

Shah, V.; Von Weltin, E.; Lopez, S.; McHugh, J. R.; Veloso, L.; Golmohammadi, M.; Obeid, I.; and Picone, J. 2018. The temple university hospital seizure detection corpus. *Frontiers in neuroinformatics*, 12: 83.

Strodthoff, N.; Wagner, P.; Schaeffter, T.; and Samek, W. 2020. Deep learning for ECG analysis: Benchmarks and insights from PTB-XL. *IEEE Journal of Biomedical and Health Informatics*, 25(5): 1519–1528.

Su, Y.; Zhao, Y.; Niu, C.; Liu, R.; Sun, W.; and Pei, D. 2019. Robust anomaly detection for multivariate time series through stochastic recurrent neural network. In *Proceedings of the 25th ACM SIGKDD international conference on knowledge discovery & data mining*, 2828–2837.

Tang, S.; Dunnmon, J.; Saab, K. K.; Zhang, X.; Huang, Q.; Dubost, F.; Rubin, D.; and Lee-Messer, C. 2021. Self-Supervised Graph Neural Networks for Improved Electroencephalographic Seizure Analysis. In *International Conference on Learning Representations*.

Tang, S.; Dunnmon, J. A.; Liangqiong, Q.; Saab, K. K.; Baykaner, T.; Lee-Messer, C.; and Rubin, D. L. 2023. Modeling Multivariate Biosignals With Graph Neural Networks and Structured State Space Models. In *Conference on Health, Inference, and Learning*, 50–71. PMLR.

Wagner, D.; Michels, T.; Schulz, F. C.; Nair, A.; Rudolph, M.; and Kloft, M. 2023. TimeseAD: Benchmarking deep multivariate time-series anomaly detection. *Transactions on Machine Learning Research*.

Wei, Y.; Jang-Jaccard, J.; Xu, W.; Sabrina, F.; Camtepe, S.; and Boulic, M. 2023. LSTM-autoencoder-based anomaly detection for indoor air quality time-series data. *IEEE Sensors Journal*, 23(4): 3787–3800.

Wu, R.; and Keogh, E. 2021. Current time series anomaly detection benchmarks are flawed and are creating the illusion of progress. *IEEE Transactions on Knowledge and Data Engineering*.

Xu, K.; Hu, W.; Leskovec, J.; and Jegelka, S. 2019. How powerful are graph neural networks? In *International Conference on Learning Representations*.

Yang, Y.; Zhang, C.; Zhou, T.; Wen, Q.; and Sun, L. 2023. Dcdetector: Dual attention contrastive representation learning for time series anomaly detection. In *Proceedings of the 29th ACM SIGKDD Conference on Knowledge Discovery and Data Mining*, 3033–3045.

Zhu, Y.; Xu, W.; Zhang, J.; Du, Y.; Zhang, J.; Liu, Q.; Yang, C.; and Wu, S. 2022. A survey on graph structure learning: Progress and opportunities. In *International Joint Conference on Artificial Intelligence*.